ADVANCED FUNCTIONAL MATERIALS
www.afm-journal.de

High-Performance n-Channel Thin-Film Field-Effect Transistors Based on a Nanowire-Forming Polymer

Suk Gyu Hahm, Yecheol Rho, Jungwoon Jung, Se Hyun Kim, Tissa Sajoto, Felix S. Kim, Stephen Barlow, Chan Eon Park, Samson A. Jenekhe, Seth R. Marder and Moonhor Ree**

A new electrontransport polymer, poly{[*N*,*N*′-dioctylperylene-3,4,9,10-bis(dicarboximide)-1,7(6)-diyl]-*alt*-[(2,5-bis(2-ethyl-hexyl)-1,4-phenylene)bis(ethyn-2,1-diyl]} (PDIC8-EB), is synthesized. In chloroform, the polymer undergoes self-assembly, forming a nanowire suspension. The nanowire's optical and electrochemical properties, morphological structure, and field-effect transistor (FET) characteristics are investigated. Thin films fabricated from a PDIC8-EB nanowire suspension are composed of ordered nanowires and ordered and amorphous non-nanowire phases, whereas films prepared from a homogeneous PDIC8-EB solution consist of only the ordered and amorphous non-nanowire phases. X-ray scattering experiments suggest that in both nanowires and ordered phases, the PDIC8 units are laterally stacked in an edge-on manner with respect to the film plane, with full interdigitation of the octyl chains, and with the polymer backbones preferentially oriented within the film plane. The ordering and orientations are significantly enhanced through thermal annealing at 200 °C under inert conditions. The polymer film with high degree of structural ordering and strong orientation yields a high electron mobility (0.10 ± 0.05 cm^2 V^{-1} s^{-1}), with a high on/off ratio (3.7×10^6), a low threshold voltage (8 V), and negligible hysteresis (0.5 V). This study demonstrates that the polymer in the nanowire suspension provides a suitable material for fabricating the active layers of high-performance n-channel FET devices via a solution coating process.

Dr. S. G. Hahm, Dr. T. Sajoto, Dr. S. Barlow, Prof. S. R. Marder
School of Chemistry and Biochemistry
and Center for Organic Photonics and Electronics
Georgia Institute of Technology
Atlanta, GA 30332-0400, USA
E-mail: seth.marder@chemistry.gatech.edu

Dr. S. G. Hahm, Y. Rho, J. Jung, Prof. M. Ree
Department of Chemistry
Division of Advanced Materials Science
Pohang Accelerator Laboratory
Center for Electro-Photo Behaviors in Advanced Molecular Systems
BK School of Molecular Science, and Polymer Research Institute
Pohang University of Science & Technology
Pohang 790-784, Republic of Korea
E-mail: ree@postech.edu

Dr. S. H. Kim, Prof. C. E. Park
Department of Chemical Engineering and Polymer Research Institute
Pohang University of Science & Technology
Pohang 790-784, Republic of Korea

Dr. F. S. Kim, Prof. S. A. Jenekhe
Department of Chemical Engineering and Department of Chemistry
University of Washington
Seattle, WA 98195-1750, USA

DOI: 10.1002/adfm.201202065

1. Introduction

Solution-processable organic field-effect transistor (OFET) materials have recently attracted interest because they are potentially applicable in radio frequency identification tags, rollable displays, and large-area sensors. OFETs are easily miniaturized, and their properties can be tailored through chemical synthesis.[1–9] Significant efforts have been made toward the development of solution-processable polymeric materials for OFETs that are easily processable, flexible, display a high mechanical strength, and are scalable.[10] Several polymers have been developed for use in p-channel thin film transistors with a wide range of hole mobilities (μ_h = 0.01–8.0 cm^2 V^{-1} s^{-1});[11–18] however, polymers for use in n-channel transistors are scarce. Identified n-channel transistor polymers include the polybithiopheneimides,[19] ladder-type poly(benzobisimidazobenzophenanthroline) (BBL),[20] conjugated naphthalene diimide (NDI)-based polymers,[21–23] perylene diimide (PDI)-based polymers,[24,25] and indenofluorenebis(dicyanovinylene)-based polymer.[26] The electron mobilities, μ_e, of these polymers are generally lower than the hole mobilities μ_h of the p-channel polymers and of single crystals of small conjugated molecules.[27] Thus, the development of high-performance n-channel OFET polymers is still in the exploration stages.

Formation of charge-transporting polymer semiconductor nanowires, either prior to or after deposition of active layers, has been explored as an effective means to control the solid-state morphology of polymer thin films and, thus, to enhance the performance of OFETs.[28–30] Self-organized charge-transporting polymer nanowires are of special interest, since they can be readily processed into active layers in devices and have been shown to exhibit high field-effect mobility.[29,30] The high mobility of organic semiconductor nanowires is proposed to originate from the highly ordered molecular packing with small inter-molecular distances in the nanowire, which is driven by strong π–π attraction and aliphatic side-chain interactions. However, although the utilization of pre-assembled nanowires in an active layer is promising for achieving high charge-carrier mobility in OFETs, only few examples have been demonstrated from electron-transporting polymers.[30]

In this study, we report the fabrication and characterization of n-channel OFET devices based on nanoscale thin films formed from a new polymer, poly{[*N,N′*-dioctylperylene-3,4,9,10-bis(dicarboximide)-1,7(6)-diyl]-*alt*-[(2,5-bis(2-ethylhexyl)-1,4-phenylene)bis(ethyn-2,1-diyl]} (PDIC8-EB). This polymer was synthesized by the Sonogashira coupling reaction of *N,N′*-dioctyl-1,7(6)-dibromo-3,4,9,10-perylenebis(dicarboximide) (PDIC8) and 1,4-bis(2-ethylhexyl)-2,5-diethynylbenzene (EB) with the aid of a palladium and copper catalyst system. The PDIC8-EB polymer dissolved completely in hot chloroform under a nitrogen atmosphere. The polymer molecules formed nanowires in solution via self-assembly when the solution was incubated under dark conditions at room temperature. Nanometer-scale thin films of the polymer could be prepared either with or without nanowires, and the film structures and properties were characterized. OFET devices were fabricated from the thin polymer films with or without nanowires, for comparison purposes. The active polymer layers were further thermally annealed at various temperatures. The electronic behavior depends on the presence or absence of the polymer nanowires and the thermal annealing history; in the case of nanowire devices annealed at 200 °C, mobilities of 0.10 ± 0.05 $cm^2\ V^{-1}\ s^{-1}$ and high current on/off ratios of 10^6–10^7 were obtained. The observed device performances were evaluated in light of the polymer film morphological structures and properties.

2. Results and Discussion

The linkers in most conjugated rylene diimide polymers reported to date[21–25] have been based on thiophene materials, although arylene bridges have also been used.[31] We have been interested in the use of alkyne linkers in rylene diimide polymers since these may allow for more planar, and more rigid polymer structures, perhaps facilitating stronger interchain interactions, and have recently synthesized a series of poly{[*N,N′*-dialkyl-naphthalene-1,4,5,8-bis(dicarboximide)-2,6-diyl]-*alt*-[(1,4-arylene) bis-(ethyn-2,1-diyl]} materials.[32] The PDIC8-EB polymer that is the focus of the present work was synthesized from *N,N′*-dioctyl-1,7(6)-dibromo-3,4,9,10-perylenebis(dicarboximide) (PDIC8) and 1,4-bis(2-ethylhexyl)-2,5-diethynylbenzene (EB) via a Pd-catalyzed Sonogashira coupling reaction (**Scheme 1**; see Experimental part) in a similar fashion to its naphthalene diimide analogues.

The polymer was purified by Soxhlet extraction with multiple solvents, followed by precipitation, and was characterized by elemental analysis, gel permeation chromatography (GPC), and ^{1}H NMR spectroscopy (see the data in the Experimental part). The weight-average molecular weight ($\overline{M_w}$) and polydispersity index (PDI) were estimated to be 66 900 Da and 4.22, respectively, by GPC in chloroform. The polymer was thermally stable up to 400 °C (5% weight loss) (Supporting Information Figure S1). The polymer showed no phase transitions between room temperature and 350 °C (Supporting Information Figure S2).

Figure 1a,b show cyclic voltammograms (CVs) of PDIC8-EB, measured in solution and in a film on the working electrode, respectively. The half-wave potential for the first reduction potential in solution was –0.40 V vs ferrocenium/ferrocene. The solution-state electron affinity (EA) of the polymer was estimated to be –3.9 eV using the empirical relation, EA = $-((eE_{1/2}^{0/-} - eE(\text{ferrocene}) + 4.8\ \text{eV})$, where e is the electronic charge. A similar value was obtained from the onset potential for the solid film ($E_{\text{onset}}^{\text{red}}$ = –0.444 V) in place of the solution half-wave potential. The reduction potential of the polymer is similar to that of analogous napthalene diimide/diethynylbenzene polymers;[32] in both classes of the polymers the diethynylbenzene bridge leads to little change in the redox potential relative to that of the appropriate parent rylene diimide.[33] The thin film ionization potential (IP) was measured to be 6.1 eV by ultraviolet photoelectron spectroscopy (UPS) (Figure 1c). The CV and UPS data were used to estimate a transport gap (i.e., IP/EA energy gap) of 2.2 eV. The EA and transport gap values are similar to the values observed previously for PDI monomers and polymers[24,33,34] that act as electron-transport materials, and the EA value suggests a relatively low barrier to electron injection from common electrode materials into the polymer.

The polymer was dissolved completely in hot chloroform (80 °C) and the resulting solution was cooled to room temperature and then filtered over a filter with a 0.2-μm pore size to yield 5–10 mg mL^{-1} homogeneous solutions. The polymer solutions gave high-quality thin films via conventional spin-coating. When incubated under dark conditions at room temperature for 3 days, the originally homogeneous polymer solution underwent a self-assembly transformation to yield a nanowire suspension. The nanowire-containing suspension was considerably more viscous than the original solution. Once the nanowires were formed, they were stable even upon the addition of more chloroform (see the ultraviolet-visible (UV-vis) spectra of the diluted suspensions, shown in Supporting Information Figure S3). The nanowires remained suspended when left standing for one month. Overall, the nanowire suspension was quite stable; however, the nanowires could be dissolved upon heating to 90–100 °C. Presumably the formation of nanowires is favored by the strong tendency of PDIs to aggregate via π-stacking,[33] with the alkyne-based bridging groups offering relatively little steric hindrance to such stacking compared to the other bridging groups that may be twisted out the PDI plane, while the alkyl side chains are evidentally sufficiently longer and/or branched to solubilize the polymer, but insufficiently so to disrupt nanowire formation.

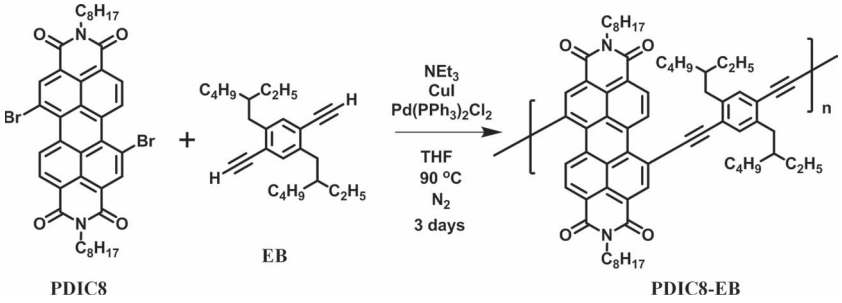

Scheme 1. Synthesis and chemical structure of PDIC8-EB.

The nanowire suspension was used to prepare thin films on silicon (Si) substrates that had been treated either with or without a silane derivative via conventional spin-coating

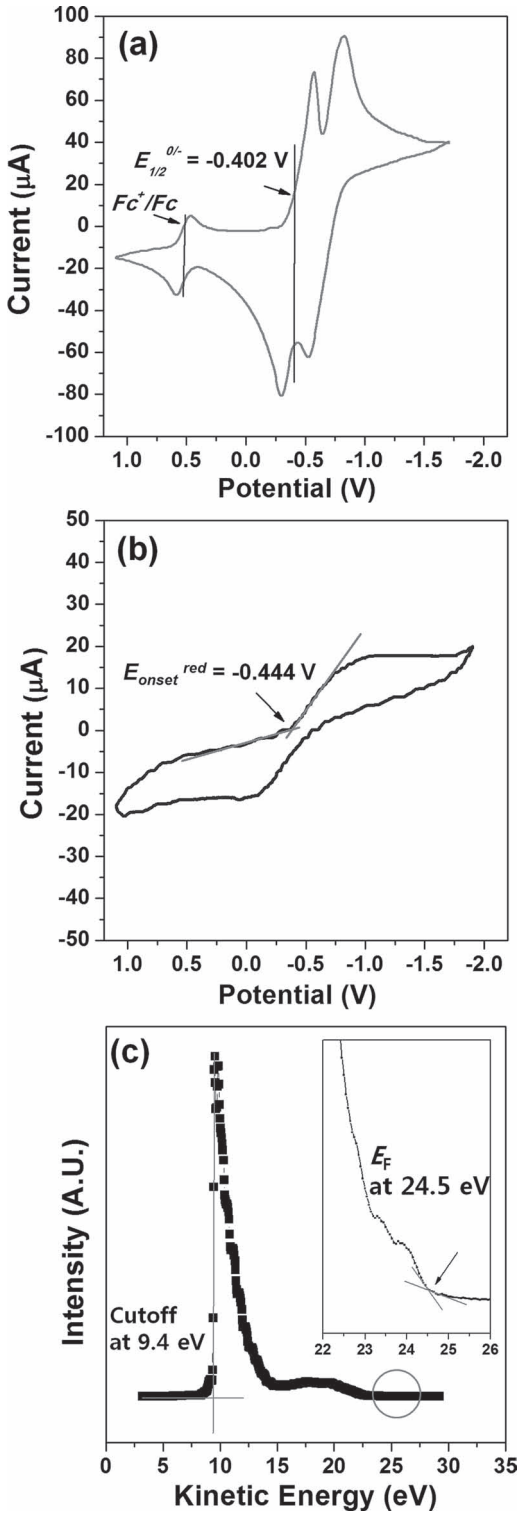

Figure 1. a) Cyclic voltammogram (CV) of PDIC8-EB in $CHCl_3$/0.1 M $[n\text{-}Bu4N]^+[PF_6]^-$ with ferrocenium/ferrocene as an internal standard, at 50 mV s^{-1}. b) CV of a film of PDIC8-EB deposited on a platinum button working electrode in acetonitrile/0.1 M $[n\text{-}Bu_4N]^+[PF_6]^-$ at 50 mV s^{-1}. The horizontal scale is relative to a AgCl-coated Ag-wire pseudo-reference electrode. c) UPS (He I) energy distribution curves of PDIC8-EB thin film taken with –5.0 V bias applied to the sample. The inset shows a magnified view of the ionization onset region.

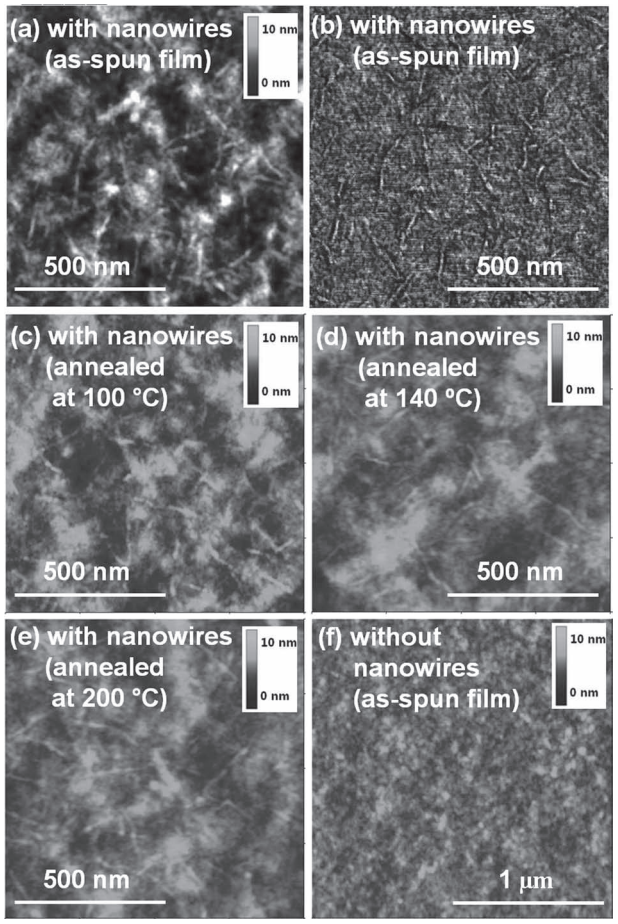

Figure 2. Representative AFM Images: a) height image (1 μm × 1 μm) of a thin film spin-coated from a PDIC8-EB nanowire suspension (10 mg mL^{-1} in $CHCl_3$); b) phase image of the film in (a). Height images (1 μm × 1 μm) of PDIC8-EB films annealed at various temperatures: c) 100 °C; d) 140 °C; and e) 200 °C. f) Height image (2 μm × 2 μm) of a film spun from a non-nanowire PDIC8-EB solution (10 mg mL^{-1} in $CHCl_3$).

processes followed by drying. Some of the as-spun films were further thermally annealed at various temperatures (100, 120, 140, 160, 180, 200, 220, and 240 °C) for 1 h in a glove box under a nitrogen atmosphere (< 0.1 ppm O_2). The polymer thin films (ca. 25-nm thick) were examined by atomic force microscopy (AFM), high-resolution transmission electron microscopy (TEM), grazing incidence X-ray scattering (GIXS), and X-ray reflectivity (XR).

Height and phase AFM images of the polymer films fabricated from the nanowire suspension are shown in **Figure 2**a,b, respectively. The AFM images clearly reveal the well-defined nanowires. The nanowires were determined to be 0.5–1 μm in length and 4–40 nm in width (Supporting Information Figure S4). The films were estimated to have a root-mean-square (rms) surface roughness of 0.895 nm over the area of 1.0 μm × 1.0 μm. This surface roughness was slightly higher than that (0.571 nm) of films prepared from the homogeneous polymer solution without nanowires (Figure 2f). The nanowire dimensions did not change in the film state upon thermal annealing up to 200 °C (Figure 2c–e).

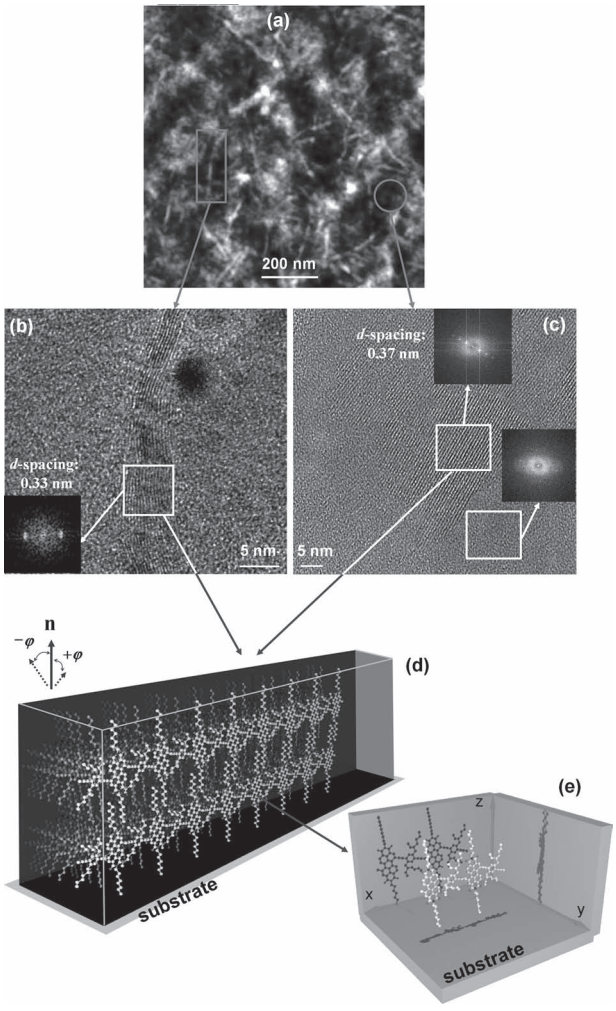

Figure 3. a) Height AFM image (1 μm × 1 μm) of a thin film spin-coated from a PDIC8-EB nanowire suspension (10 mg mL^{-1} in $CHCl_3$); b) high-resolution TEM image of a 200 °C annealed film of PDIC8-EB (the inset is the FFT pattern obtained from the data of the part of a nanowire in the square region); c) high-resolution TEM image of a 200 °C annealed film of PDIC8-EB (the inset is the FFT pattern obtained from the data of the part of an ordered phase in the square region). d) A model of the multibilayer-structured PDIC8-EB molecules proposed from the TEM and GIXS measurements and data analyses; e) a molecular model of a PDIC8-EB polymer chain in the multibilayer structure. **n** is the orientation vector for the multibilayer-structured PDIC8 units with respect to the out-of-plane of the film where φ is the polar angle between the **n** vector and the out-of-plane of the film.

The films containing nanowires annealed at 200 °C were further examined by high-resolution transmission electron microscopy (TEM). TEM images were collected and analyzed in light of the AFM results discussed above. TEM analysis confirmed the presence and absence of nanowires in various regions, consistent with the results obtained from the AFM (**Figure 3**a,b). TEM analysis further found that the annealed films included two different phases without nanowires, one ordered and one apparently amorphous, in addition to the nanowire phase (Figure 3b,c). The nanowires consisted of layer stacks with an interpolymer distance of 0.33 nm (Figure 3b).

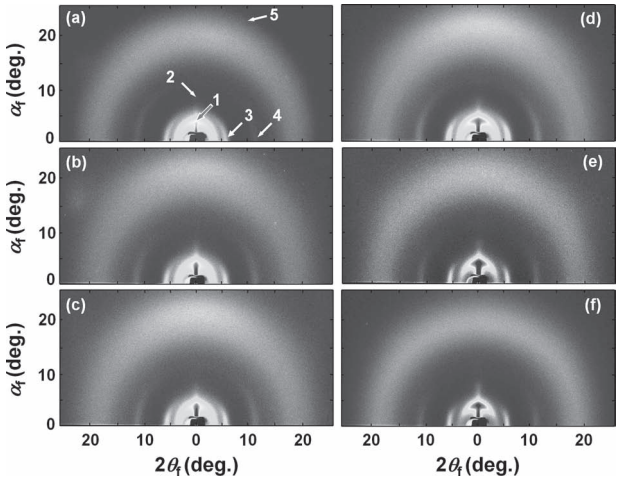

Figure 4. 2D GIXS patterns of PDIC8-EB films (which were prepared with a PDIC8-EB nanowire suspension (10 mg mL^{-1} in $CHCl_3$)) before and after thermal annealing at various temperatures in a glove box under nitrogen atmosphere: a) 25 °C; b) 100 °C; c) 120 °C; d) 160 °C; e) 200 °C; and f) 240 °C. The measurements were carried out at an incident angle $\alpha_i = 0.160°$.

The interlayer distance is in the range of expected π-stacking distances and is, therefore, consistent with an interpolymer distance between polymer chains in an extended sheet conformation, suggesting that the nanowire was composed of polymer sheets. Similar layer stacks were also observed in the ordered phase without nanowires, the area of which was 5–15 nm by 5–35 nm (Figure 3c), but with a slightly larger interlayer distance of 0.37 nm, suggesting less dense packing of the polymer sheets than in the nanowires. The remaining phase without nanowires was apparently featureless and was, therefore, considered to be amorphous (Figure 3b,c).

The TEM images of films prepared from the PDIC8-EB solution without nanowires also revealed both ordered and amorphous phases (Supporting Information Figure S5). The ordered phases were similar in shape to those observed in films prepared from the PDIC8-EB nanowire suspension. The layer stacks in such ordered phases displayed an interlayer distance of 0.40 nm, slightly larger than that observed in films prepared from a PDIC8-EB nanowire suspension.

In view of the results described above, the films were further investigated by synchrotron GIXS analysis. The as-spun films (which were fabricated from the nanowire suspension) revealed a two-dimensional (2D) GIXS pattern (**Figure 4**a). The 2D GIXS pattern showed arc and anisotropic ring scatterings (marked as 1, 2, 3, and 4) in the low-angle region, suggesting that in the film, the polymer chains formed an ordered structure; however, the polymer orientations were somewhat distributed. Similar GIXS patterns were observed for films prepared from a PDIC8-EB solution without nanowires (Supporting Information Figure S6), indicating that in both types of films a significant proportion of ordered phases is present, consistent with the TEM analysis described above.

The arc and anisotropic ring scatterings became sharper in intensity and smaller in size upon thermal annealing (Figure 4b–f),

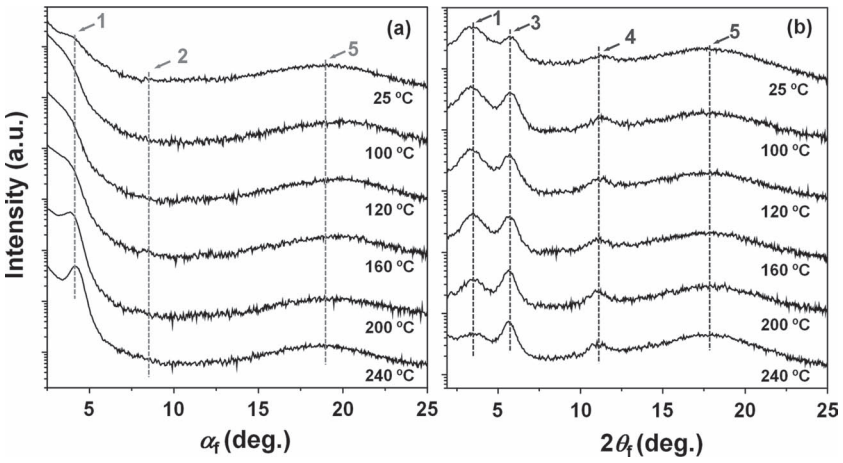

Figure 5. a) Out-of-plane scattering profiles extracted from the 2D GIXS patterns in Figure 4 along the α_f direction at $2\theta_f = 0.0°$; b) in-plane scattering profiles from the 2D GIXS patterns in Figure 4 along the $2\theta_f$ direction at $\alpha_f = 0.160°$.

suggesting that the structures in the films became more ordered and preferentially oriented under thermal annealing.

The scattering data were further analyzed by extracting the out-of-plane and in-plane scattering profiles from the 2D GIXS patterns along the α_f-direction at $2\theta_f = 0°$ and the $2\theta_f$-direction at $\alpha_f = 0.160°$, respectively (**Figure 5**a,b).

For the as-spun films, the scattering peaks 1 and 2 appeared at $\alpha_f = 3.93°$ and 7.86° (Figure 4a and Figure 5). The relative peak positions from the specular reflection indicated that the peaks 1 and 2 were first- and second-order reflections, respectively. Peak 1 was relatively strong in intensity. In contrast, peak 2 was very weak and, thus, not easily discernible. The intensity of peak 1 was stronger in the out-of-plane scattering profile than in the in-plane scattering profile. In the out-of-plane scattering profile, the intensity of peak 1 was significantly stronger upon thermal annealing at higher temperatures, up to 240 °C (Figures 4 and Figure 5a). For the in-plane scattering profile, the intensity of peak 1 was stronger upon thermal annealing until a temperature of 160 °C, but the intensity decreased dramatically upon thermal annealing at temperatures 200 °C and higher (Figures 4 and Figure 5b).

The *d*-spacing of peak 1 was determined to be 2.01 nm, which is equivalent to two-thirds of the length of the major axis of the PDIC8 unit with the two *n*-octyl side groups in a fully extended conformation, according to molecular simulations using the Cerius^2 software (Accelrys, San Diego, CA, USA). Moreover, the molecular simulations reveal that one-third of this major axis dimension correspond to the length of the planar PDI core, with each fully extended *n*-octyl group contributing another third. Thus, these results collectively are fully consistent with an ordered phase (i.e., nanowire phase and ordered non-nanowire phase) in which the *n*-octyl side groups are fully interdigitated with those in adjacent PDIC8 units, with the 2.01 nm repeat distance corresponding to the interpolymer repeat distance in the polymer plane. The GIXS measurements showed that the ordering and orientations of such multibilayer-structured PDIC8 units were enhanced by thermal annealing; the enhancements depended on the annealing temperature.

To get more detailed information about the degree of ordering and orientation of the PDIC8 units in the above-mentioned interdigitated structure, an azimuthal profile of the peak 1 was extracted from each 2D GIXS pattern in Figure 4 and then analyzed. The obtained azimuthal profiles are displayed together in **Figure 6** as a function of azimuthal angle μ. The azimuthal scattering intensity *IGIXS*, $\varphi(\mu)$ can be obtained by averaging $I_{GIXS}(\mu)$ over possible orientations of the multibilayer structured PDIC8 unit:[35]

$$I_{GIXS,\varphi}(\mu) = \int_{-\pi}^{\pi} I_{GIXS}(\mu)\, D(\varphi) d\varphi \quad (1)$$

where $D(\varphi)$ is a distribution function of the orientation vector **n** for the multibilayer structured PDIC8 unit with respect to the out-of-plane of the film, where φ is the polar angle between the **n** vector and the out-of-plane of the film. The second order orientation factor O_s (which is a measure of the orientation of the multibilayer structured PDIC8 unit) can be defined as the following equation:[35,36]

$$O_s = \int D(\varphi) \frac{(3\cos^2\varphi - 1)}{2} d\varphi. \quad (2)$$

When $D(\varphi)$ is strongly peaked around $\varphi = 0$ (i.e., vertical orientation), $\cos\varphi = 1$ and $O_s = 1$; on the other hand, if the orientation is entirely random, $<\cos^2\varphi = 1/3$ and $O_s = 0$. All

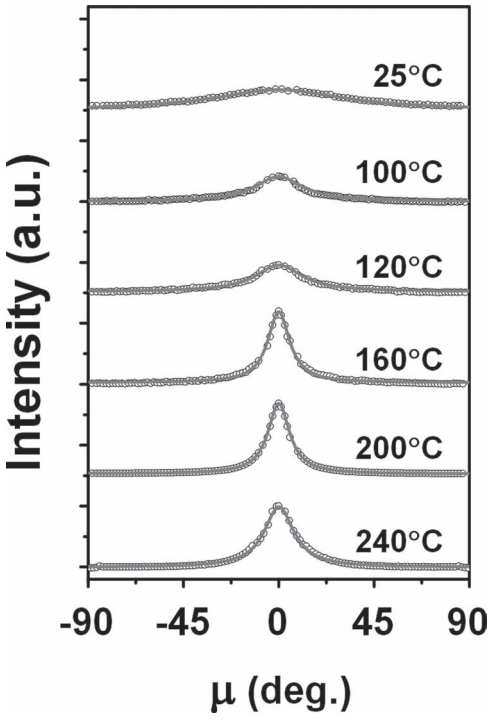

Figure 6. Azimuthal scattering profiles of the peak 1 from the GIXS patterns in Figure 4.

Table 1. Data for scattering peak 1 in the two-dimensional GIXS patterns measured for the PDIC8-EB films deposited on silicon substrates before and after thermal annealing for 1 h at various temperatures.

Polymer Film	Peak 1			Orientation		
Annealing Temperature [°C]	$I_{max(\mu=0°)}$ [a]	$I_{min(\mu=\pm90°)}$ [b]	R [c]	$\overline{\varphi}$ [d] [deg]	$\gamma\varphi$ [e] [deg]	O_s [f]
25 [g]	45.7	15.2	3.0	0	126.2	0.12
25 [h]	333.7	58.7	5.7	0	78.4	0.21
100 [i]	410.1	10.4	39.4	0	27.3	0.51
120 [i]	435.5	10.7	40.7	0	27.0	0.51
160 [i]	1156.0	8.5	136.8	0	16.7	0.65
200 [i]	2205.6	10.4	212.1	0	11.9	0.73
240 [i]	1489.5	13.1	114.1	0	17.1	0.64

[a] The intensity at the peak maximum in the azimuthal scattering profile of the peak 1, which corresponded to the intensity at an azimuthal angle μ of 0° (Figure 6). [b] The intensity at the peak minimum in the azimuthal scattering profile of the peak 1, which corresponded to the intensity at an azimuthal angle μ of ±90° (Figure 6). [c] $I_{max(\mu=0°)}/I_{min(\mu=\pm90°)}$. [d] The mean orientation angle; here the orientation angle ϕ is defined by the polar angle between the orientation vector **n** and the out-of-plane of the film where the vector **n** is given for the multibilayer structured PDIC8 unit with respect to the out-of-plane of the film. [e] The half-width at the half-maximum (HWHM) of orientation distribution. [f] Orientation factor, which the second order orientation factor, a measure of the orientation of the multibilayer structured PDIC8 unit. [g] The as-spun film fabricated from a PDIC8-EB solution without nanowires. [h] The as-spun film fabricated from the PDIC8-EB nanowire suspension. [i] The film was fabricated from the PDIC8-EB nanowire suspension and then thermally annealed at a given temperature for 1 h in inert condition.

the azimuthal scattering profiles showed a maximum intensity at $\mu = 0°$ and a minimum at $\mu = 90°$ and −90° (Figure 6). These scattering profiles were found to be satisfactorily fitted by using eq 1 with Cauchy–Lorentz distribution function:

$$D(\varphi) = \frac{1}{\pi}\left[\frac{\gamma_\varphi}{(\varphi-\overline{\varphi})^2+\gamma_\varphi^2}\right]. \quad (3)$$

where $\overline{\varphi}$ is the mean angle and $\gamma\varphi$ is the half-width at the half-maximum (HWHM) of φ from $\overline{\varphi}$. The orientation analysis results, as well as the maximum and minimum scattering intensities ($I_{max(\mu=0°)}$ and $I_{min(\mu=\pm90°)}$) and their ratio R are summarized in **Table 1**.

Peak 1 for the as-spun film (which was prepared from the PDIC8-EB nanowire suspension) in the azimuthal profile was very weak and broad. This weak broad scattering peak yielded the following values: R = 5.7 (= $I_{max(\mu=0°)}/I_{min(\mu=\pm90°)}$ = 333.7/58.7), $\overline{\varphi}$ = 0°, $\gamma\varphi$ = 78.4°, and O_s = 0.21, confirming that the interdigitated multi-bilayers of PDIC8 units were preferentially aligned along the out-of-plane direction of the film, but the orientation angle distribution was broad. The multibilayer-structured PDIC8 units in the as-spun film prepared from the PDIC8-EB solution without nanowires were also found to be preferentially oriented along the out-of-plane direction of the film, but with a much broader orientation distribution: R = 3.0 (= 45.7/15.2), $\overline{\varphi}$ = 0°, $\gamma\varphi$ = 126.2°, and O_s = 0.12) (Table 1). The peak intensity was one-seventh the intensity of the corresponding peak for a film prepared from the PDIC8-EB nanowire suspension, indicating that both the degree of ordering and the population of the multi-bilayered structure were much lower in the film prepared from the PDIC8-EB solution without nanowires than in the film prepared from the PDIC8-EB nanowire suspension.

The intensity of peak 1 was higher and sharper after thermal annealing. The maximum peak intensity gradually increased with increasing annealing temperature until 120 °C, after which point the peak intensity dramatically increased with further increases in the annealing temperature up to 200 °C. Annealing at temperatures beyond 200 °C, however, yielded lower maximum peak intensities (Figure 6 and Table 1). These collectively indicate that the degree of ordering, orientation and population of the multi-bilayered PDIC8 units in the film were significantly enhanced via thermal annealing process. The highest degree of ordering was achieved upon annealing at 200 °C. The orientation factor O_s dramatically increased to 0.73 and the orientation distribution was relatively small ($\gamma\varphi$ = 11.9°) for the film annealed at 200 °C, in comparison to the as-spun film with an O_s of 0.21 and a $\gamma\varphi$ of 78.4°.

Peaks 3 and 4 appeared at $2\theta_f$ = 5.75° (d-spacing = 1.38 nm) and 11.45° (d-spacing = 0.69 nm), respectively (Figure 4a and Figure 5). These peaks were clearly detected in the in-plane scattering profile but were not discernible in the out-of-plane scattering profile. The intensities of both peaks strengthened and the shapes grew sharper upon thermal annealing at higher temperatures (Figure 5b). The relative specular reflection peak positions indicated that peak 4 was the second-order reflection of peak 3. The d-spacings of the first order peak (peak 3) agreed well with the length of the chemical repeat unit along the polymer backbone according to the Cerius^2 software. Based on this assignment, the data indicate that the ordered polymer backbones are preferentially aligned in the plane of the film. The polymer backbone ordering increased upon thermal annealing, but the enhancement depended on the annealing temperature. The highest ordering and in-plane orientations of the polymer backbones were observed in the film annealed at 200 °C.

In addition to the arc and anisotropic peaks discussed above, the as-spun film showed a very broad scattering ring (i.e., peak 5) over the range 10–27° (Figure 4 and Figure 5). The peak maximum appeared at 19.41° (d-spacing = 0.41 nm) in the out-of-plane scattering profile and at 17.93° (d-spacing = 0.44 nm) in the in-plane scattering profile. The very broad peaks and relatively short d-spacing permitted the ring scattering patterns to be assigned as reflections from the polymer chains and side groups separated by a distribution of interpolymer distances. The d-spacing for the out-of-plane scattering profile was slightly smaller than that for the in-plane scattering profile, indicating that overall, the polymer chains were packed somewhat more closely along the out-of-plane direction of the film than along the film plane. Slight packing differences in the polymer chains may be attributed to the preferential in-plane orientations of the polymer backbone in the nanometer-scale thin film. The ring scattering pattern positions did not vary significantly upon thermal annealing.

The structural information described above was used to develop a molecular packing model of the polymer chains in the nanowires and ordered phases, as shown in Figure 3d,e.

The polymer films prepared from the PDIC8-EB nanowire suspension were investigated by synchrotron X-ray reflectivity (XR) analysis. The polymer films submitted to XR analysis were

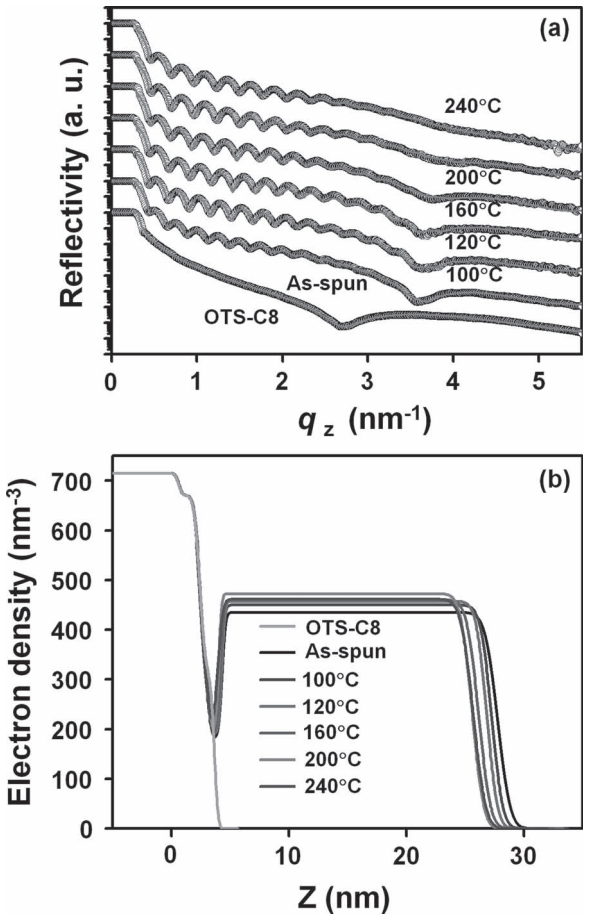

Figure 7. a) Representative XR profiles of an OTS-C8 layer coated onto a silicon substrate and PDIC8-EB films (which were prepared with a PDIC8-EB nanowire suspension (10 mg mL^{-1} in $CHCl_3$)) on the OTS-C8 treated silicon substrates before and after thermal annealing at various temperatures in a glove box under nitrogen atmosphere. The symbols are the measured data and the solid line represents the fit curve assuming a homogeneous electron density distribution within the film. b) Electron density profiles across the OTS-C8 layer alone and the polymer film layer in contact with the OTS-C8 layer, which were determined from the analysis of the data in (a).

prepared on Si substrates treated with *n*-octyltrichlorosilane (OTS-C8) in order to obtain information about the silane-polymer interface structure present in OFET devices. The OTS-C8-treated Si substrates were also examined by XR analysis. The XR data are shown in **Figure 7**a. All XR data could be fit using Parratt's fitting algorithm[37] (Figure 7a). The analysis results are provided in Figure 7b and **Table 2**.

The OTS-C8 layer deposited onto the silicon substrate had an overall electron density ρ_e of 300 nm^{-3} and a thickness d of 1.18 nm. The XR analysis results showed that the OTS-C8 monolayer consisted of two sublayers, a silicon-rich layer (ρ_e = 830 nm^{-3}, d = 0.22 nm) and a hydrocarbon (i.e., alkyl)-rich layer (ρ_e = 178 nm^{-3}, d = 0.96 nm). Here, the silicon-rich layer thickness agreed with the value estimated based on molecular simulations using the Cerius^2 software; however, the alkyl-rich layer thickness was slightly lower than the length of 1.03 nm) for the *n*-octyl groups linked to silicon in the fully extended confirmation, as estimated by molecular simulations. The results suggest that the self-assembled OTS-C8 monolayer that formed on the silicon substrate featured alkyl groups that were tilted by ca. 21° with respect to the normal direction of the substrate plane.

The as-spun PDIC8-EB films (which were coated onto the OTS-C8-treated silicon substrates) were characterized as having ρ_e = 435 nm^{-3}, d = 23.45 nm, and a surface roughness σ of 0.85 nm. This surface roughness σ value agrees well with the value obtained from AFM analysis.

The polymer film was modeled including an interfacial layer with ρ_e = 177 nm^{-3}, d = 0.97 nm, and σ = 0.30 nm in contact with the bottom OTS-C8 layer. The alkyl-rich sublayer was characterized as having ρ_e = 146 nm^{-3} and d = 0.70 nm. Here, the ρ_e value was lower and the d value was slightly smaller than the values obtained prior to the top polymer layer deposition. These results suggested that the PDIC8-EB polymer molecules, particularly the alkyl side groups, interacted favorably with the *n*-octyl-rich sublayer in the self-assembled OTS-C8 bottom layer during polymer solution coating and the subsequent drying process. As a result, the polymer alkyl side groups and the bottom layer *n*-octyl groups may have partially interdigitated to form a thin interfacial layer, which disrupted the packing structure of the self-assembled bottom layer (the alkyl-rich sublayer).

All layers in the film showed an increase in the electron density ρ_e upon thermal annealing at temperatures up to 200 °C. Annealing at temperatures beyond 200 °C resulted in a decrease in the ρ_e value. The thickness of the alkyl-rich sublayer in the OTS-C8 layer did not vary significantly upon thermal annealing. By contrast, the thickness of the other layers depended on the thermal annealing history. The XR analysis results indicated that the polymer layer and the interfacial layer in contact with the alkyl-rich OTS-C8 sublayer underwent densification (i.e., better ordering) through thermal annealing. The highest degree of ordering was observed after thermal annealing at 200 °C. The results are consistent with the scattering analysis, as described above.

Bottom-gate and bottom-contact (BGBC) OFET devices (Supporting Information Figure S7a) were fabricated from the PDIC8-EB nanowire suspension or from the PDIC8-EB solution without nanowires. Devices with a bottom silicon gate electrode and gold source-drain contacts were fabricated on Si substrates with a SiO_2 insulating layer, which were treated with OTS-C8 to render the surface hydrophobic. The device performance was investigated before and after thermal annealing at a given temperature for 1 h in nitrogen atmosphere. All devices behaved as n-channel OFETs, with no measurable p-channel behavior. The as-prepared BGBC OFET devices fabricated from the PDIC8-EB nanowire suspension exhibited typical n-channel behavior with an electron mobility, μ_e, of 8.6×10^{-3} cm^2 V^{-1} s^{-1}, an on/off ratio, I_{on}/I_{off}, of 1.0×10^5, and a threshold voltage, V_{th}, of 33 V over a large source–drain V_{ds} up to 80 V bias (Supporting Information Figure S7 and Table S1). Both μ_e and I_{on}/I_{off} were improved by a factor of two upon thermal annealing at temperatures exceeding 100–180 °C; however, V_{th} did not vary significantly with thermal annealing (Supporting Information Table S1).

The as-prepared BGBC devices fabricated using the PDIC8-EB solution without nanowires displayed relatively poor

Table 2. Structural parameters and electron density profiles of PDIC8-EB films deposited on the OTS-C8 treated silicon substrates before and after thermal annealing at various temperatures[a].

Thermal annealing temperature [°C]	OTS-C8 layer						Interfacial layer			PDIC8-EB layer		
	Si-rich layer			Alkyl-rich layer								
	$d^{b)}$ [nm]	$\rho_e^{c)}$ [nm^{-3}]	$\sigma^{d)}$ [nm]	$d^{b)}$ [nm]	$\rho_e^{c)}$ [nm^{-3}]	$\sigma^{d)}$ [nm]	$d^{b)}$ [nm]	$\rho_e^{c)}$ [nm^{-3}]	$\sigma^{d)}$ [nm]	$d^{b)}$ [nm]	$\rho_e^{c)}$ [nm^{-3}]	$\sigma^{d)}$ [nm]
25[e)]	0.22	830	0.5	0.96	178	0.09						
25	0.22	830	0.5	0.70	146	0.20	0.97	177	0.30	23.45	435	0.85
100	0.22	830	0.5	0.69	153	0.32	0.94	183	0.24	22.96	450	0.75
120	0.22	830	0.5	0.70	160	0.38	0.92	191	0.21	22.53	457	0.72
160	0.22	830	0.5	0.70	165	0.33	0.90	193	0.21	21.92	460	0.80
200	0.22	830	0.5	0.70	165	0.19	0.74	196	0.21	21.34	472	0.77
240	0.22	830	0.5	0.65	160	0.22	0.68	178	0.37	21.72	465	0.83

[a)]Annealed at a given temperature for 1 h in a glove box under nitrogen atmosphere. [b)]Layer thickness. [c)]Electron density of layer. [d)]Roughness of layer in contact with air, lower or upper layer. [e)]OTS-C8 treated silicon substrate before PDIC8-EB polymer coating.

performances: $\mu_e = 5.1 \times 10^{-4}$ cm^2 V^{-1} s^{-1}, $I_{on}/I_{off} = 4.8 \times 10^3$, and $V_{th} = 16$ V. The μ_e and I_{on}/I_{off} values also improved upon thermal annealing, although the values were one order of magnitude lower than those of devices fabricated using the PDIC8-EB nanowire suspension (Supporting Information Table S1). V_{th} was found to be 16 V, which corresponded to approximately one-half of the value typically measured for devices fabricated using a PDIC8-EB nanowire suspension. V_{th} decreased significantly upon thermal annealing. These results indicate that, overall, the BGBC OFET devices fabricated using the PDIC8-EB nanowire suspension performed much better in terms of mobility and on/off ratio than OFET devices prepared using the PDIC8-EB solution without nanowires. On the other hand the devices prepared using the PDIC8-EB solution without nanowires exhibited lower V_{th} values. These may indicate better physical interaction with the bottom gate dielectric and/or with the source-drain contacts than in the devices prepared from the PDIC8-EB nanowire suspension. However, poorer contacts would also be expected to adversely affect mobility, suggesting either that the interactions with the dielectric are responsible. Such contacts improved upon thermal annealing at temperatures up to 150 °C, although thermal annealing at 180 °C did little to improve V_{th}.

Bottom-gate and top-contact (BGTC) OFET devices (**Figure 8**a) were also fabricated from the PDIC8-EB nanowire suspension. The devices were fabricated on SiO_2/Si substrates with surfaces that had been pretreated with OTS-C8 or hexamethyldisilazane (HMDS). SiO_2/Si substrates without silane-derivative treatment were also used for device

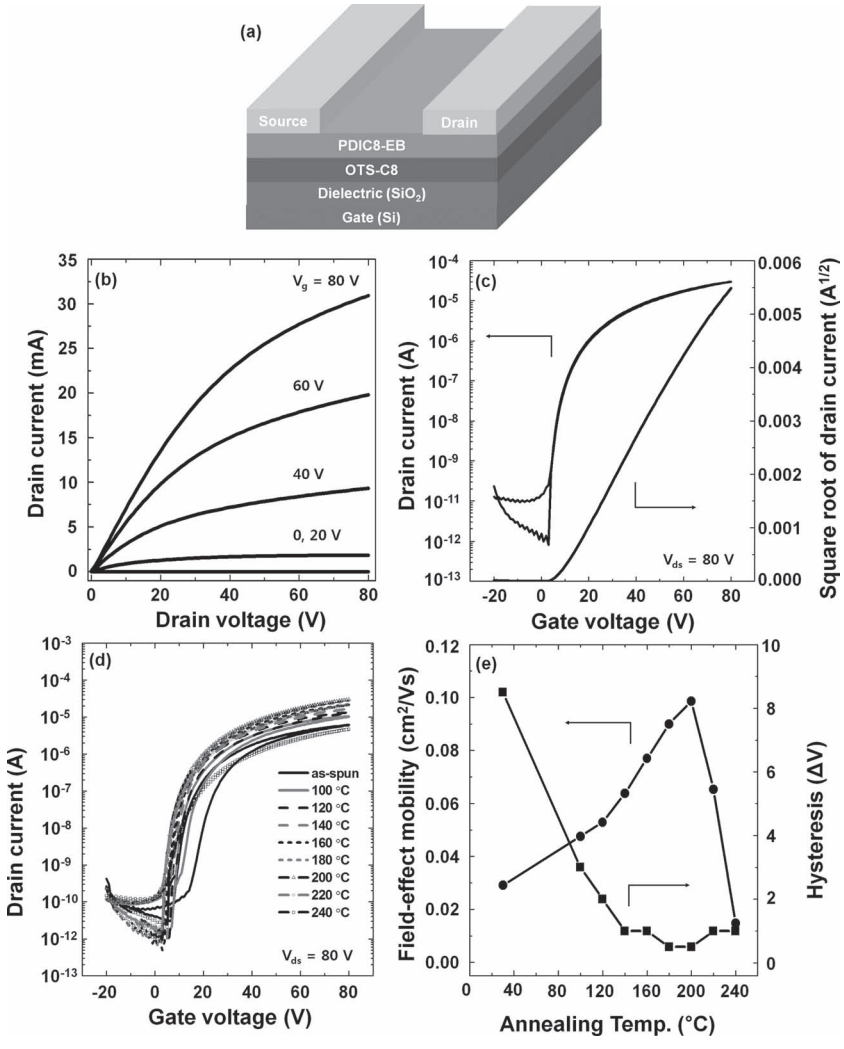

Figure 8. a) Schematic structure of BGTC OFET devices; b) output curves and c) transfer curves of the PDIC8-EB based OFETs devices annealed at 200 °C for 1 h in a glove box under nitrogen atmosphere; d) transfer curves of the PDIC8-EB based OFETs devices annealed at various temperatures for 1 h in a glove box under nitrogen atmosphere; e) field-effect electron mobility μ_e and hysteresis (ΔV) at 1.0×10^{-8} A which were obtained from the *I*–*V* data in (d).

Table 3. Performance of the bottom-gate and top-contact (BGTC) OFET devices (which were fabricated with the PDIC8-EB nanowire suspension) before and after thermal annealing at various temperatures.[a)]

Thermal annealing temperature [°C]	Device characteristics			
	μ_e[b)] [$cm^2 V^{-1} s^{-1}$]	I_{on}/I_{off}[c)]	V_{th}[d)] [V]	Hysteresis ΔV[e)] [V]
As-fabricated	3.0 (±0.3) × 10^{-2}	2.0 (±0.1) × 10^5	10 (±0.2)	8.5 (±0.1)
100	4.6 (±0.3) × 10^{-2}	8.3 (±0.3) × 10^5	9 (±0.1)	3.0 (±0.1)
120	5.3 (±0.2) × 10^{-2}	1.6 (±0.1) × 10^6	8 (±0.1)	2.0 (±0.1)
180	9.0 (±0.2) × 10^{-2}	3.9 (±0.2) × 10^6	8 (±0.2)	0.5 (±0.1)
200	1.0 (±0.5) × 10^{-1}	3.7 (±0.1) × 10^6	8 (±0.1)	0.5 (±0.1)
240	1.5 (±0.6) × 10^{-2}	2.3 (±0.1) × 10^6	9 (±0.1)	1.0 (±0.1)

[a)]Annealed at a given temperature for 1 h in a glove box under nitrogen atmosphere. [b)]Average electron mobility. [c)]The current on-off ratio determined from the current at V_g = 80 V (I_{on}) and the minimum current at $V_g \approx -20$ to 3 V (I_{off}). [d)]Threshold voltage. [e)]The I_{ds}–V_g hysteresis measured at I_{sd} of 1 × 10^{-8} A (V_{sd} = 80 V) in transfer curves between off-to-on and on-to-off sweeps of the device.

fabrication, for comparison purposes. Representative device performance data are shown in Supporting Information Figure S8. The OTS-C8 treated devices performed much better than the other devices. The alkyl groups of the OTS-C8 were analogous to the side groups in the PDIC8 units of the active PDIC8-EB polymer, providing good affinity for the active polymer layer in the device (as confirmed by the XR analysis discussed above). The OTS-C8-treated devices performance was further investigated before and after thermal annealing at a selected temperature for 1 h in a glove box under a nitrogen atmosphere (< 0.1 ppm O_2). Representative current–voltage data are shown in Figure 8b–d. The device performance analysis results are summarized in Figure 8e and **Table 3**.

The as-prepared devices were characterized as having the following values: μ_e = 3.0 × 10^{-2} cm^2 V^{-1} s^{-1}, I_{on}/I_{off} = 2.5 × 10^5, V_{th} = 10 V and a hysteresis, ΔV, of 8.0 V (Figure 8e and Table 3). Here, ΔV is the I_{sd}–V_g hysteresis defined as the voltage difference at a source-drain current I_{sd} of 1 × 10^{-8} A (V_{sd} = 80 V) in the transfer curves between the off-to-on and on-to-off sweepings of the device, where V_g is the gate voltage. The BGTC device performed much better than unannealed BGBC devices fabricated using the same PDIC8-EB nanowire suspension and comparably to thermally annealed BGBC PDIC8-EB nanowire devices. V_{th} for the BGTC device was only one-third to one-fourth the value observed for the BGBC devices prepared with PDIC8-EB nanowires. These results indicate that the PDIC8-EB-based OFET device performance depended strongly on the device structure and fabrication process. Better device performance characteristics may result from better interfacial contacts between the active polymer layer and the electrodes. In particular, gold deposition onto the active polymer layer during BGTC device fabrication may yield better interfacial contact than are obtained by depositing the polymer onto gold in BGBC device fabrication.

We investigated the stability in air of the BGTC devices fabricated using the PDIC8-EB nanowire suspension. For this investigation, the devices were first thermally annealed at 120 °C for 1 h in nitrogen atmosphere. Devices were then tested before and after exposure to air. The device tests were also conducted in ambient air. The test results are shown in Supporting Information Figure S9. The first sweep test run in a nitrogen atmosphere prior to air exposure revealed μ_e = 0.049 cm^2 V^{-1} s^{-1}, V_{th} = 10 V, and ΔV = 2 V (= 10–12 V) (i.e., *I*–*V* hysteresis). The second sweep test run in ambient air after exposure to air for 24 h revealed μ_e = 0.022 cm^2 V^{-1} s^{-1}, V_{th} = 37 V, and ΔV = 19 V (= 27–42 V). The third sweep test run under a nitrogen atmosphere after exposure to air for 24 h revealed μ_e = 0.031 cm^2 V^{-1} s^{-1}, V_{th} = 25 V, and ΔV = 8 V (= 43–51 V). Overall, the device performance varied, depending on the exposure to air and the test conditions (nitrogen atmosphere versus ambient air). The devices functioned better under inert conditions than in ambient air. The device performance was not fully recovered, even though the devices were operated under inert conditions after exposure to air. This result is consistent with the electrochemically estimated EA value of the polymer, which is lower in magnitude than the generally recognized threshold for air-stable n-channel operation.[38,39]

Interestingly, the BGTC OFET device performance improved significantly upon thermal annealing at higher temperatures up to 200 °C (Figure 8e and Table 3). A maximum electron mobility of 0.10 ± 0.05 cm^2 V^{-1} s^{-1} was achieved, along with a high on/off ratio (3.7 × 10^6) for devices annealed at 200 °C. This μ_e value was remarkably high compared to the values (0.001–0.06 cm^2 V^{-1} s^{-1}) for the n-channel BGTC NDI- and PDI-based polymer FET devices reported thus far.[19–21,24,25]

For the 200 °C annealed devices, we further attempted to investigate electron mobility in the linear regime (i.e., low lateral electric field region), in addition to the saturation electron mobility μ_e. The I_{sd} data were extracted at 3.0 V in the linear regime from the output curves (Figure 8b) and plotted with a function of V_g (Supporting Information Figure S10). The data analysis gave a linear electron mobility $\mu_{e,l}$ of 7.4 × 10^{-2} cm^2 V^{-1} s^{-1}. The obtained $\mu_{e,l}$ value was relatively lower than the μ_e value. This result implies that there is contact resistance at the interface of PDIC8-EB layer and source-drain channels in the device under low lateral electric field in the linear region and that electron injection can be assisted by high lateral electric field under saturation conditions.

Overall, the excellent performance of PDIC8-EB-based BGTC devices may result from the edge-on molecular stacking in the active film layer with partial interdigitation among the alkyl side groups and the in-plane backbone orientations of the PDIC8-EB molecules. These properties were achieved through nanowire formation and appropriate thermal annealing, as discussed in the AFM, TEM, GIXS, and XR analysis sections. The highest ordering and in-plane orientations of the PDIC8-EB molecules were obtained by thermal annealing at 200 °C, yielding high electron mobilities in the devices.

3. Conclusions

PDIC8-EB (an n-channel polymer that is thermally stable up to 400 °C) was synthesized with a reasonably high molecular weight via the Sonogashira coupling reaction of PDIC8 and EB. The resulting polymer was soluble in common organic solvents and yielded high-quality thin films through conventional

spin-coating process. In chloroform, the polymer molecules underwent self-assembly at room temperature to form nanowires, producing a PDIC8-EB nanowire suspension. Analysis of the optical and electrochemical properties revealed that the polymer exhibited a relatively high EA value (ca. 3.9 eV) and a large transport gap (2.2 eV).

Nanometer-scale films of the polymer were prepared from both a nanowire suspension and from a homogeneous solution, and the film structures were investigated by AFM, TEM, GIXS, and XR analysis. The films prepared from the nanowire suspension included three phases (an ordered nanowire phase and ordered and amorphous non-nanowire phase) whereas the homogeneous solution yielded only two phases (the ordered and amorphous phases). The population of the ordered phase was higher in the film prepared from the nanowire suspension than in the film prepared from the homogeneous solution. The nanowires were composed of molecularly multibilayer-structured polymer chains oriented in such a way that the PDIC8 units were laterally stacked together in an edge-on manner with respect to the film plane and the backbones were preferentially oriented along the film plane. The multibilayer structures displayed full interdigitation among the *n*-octyl side groups of the PDIC8 units of adjacent layers. The ordered phases displayed structures similar to those observed for the nanowires; however, the molecular packing density was slightly lower than that of the nanowires. The degree of ordering and the orientations of the multibilayer structures were enhanced by thermal annealing; however, the enhancements depended on the annealing temperature. The highest ordering and degree of orientation were achieved by thermal annealing at 200 °C. The 200-°C-annealed film revealed the highest electron density measured here. The polymer film also made better contact with the self-assembled OTS-C8 monolayer (deposited onto the SiO_2/Si substrate) through favorable interactions between the alkyl groups of the polymer and the silane derivative.

The highly ordered multibilayer structure and its high degree of orientation resulted in an excellent device performance for OFET devices prepared using the polymer as an active layer. The electron mobility μ_e was 0.10 ± 0.05 $cm^2\ V^{-1}\ s^{-1}$, with a high on/off ratio (3.7×10^6), for the BGTC device prepared with the 200 °C annealed polymer film (prepared from the nanowire suspension). Finally, the active polymer layer displayed a relatively low threshold voltage V_{th} (8 V) and negligible hysteresis ΔV (0.5 V).

Overall, the present findings demonstrate that PDIC8-EB polymer nanowires provide a suitable active material for the fabrication of active layers in high-performance n-channel OFET devices via a simple solution coating process.

4. Experimental Section

Materials: SII chemicals were purchased from Aldrich and used without further purification unless stated otherwise.

Synthesis of N,N′-Dioctyl-1,7(6)-dibromoperylene-3,4,9,10-bis(dicarboximide) (PDIC8). 1,7-Dibromoperylene-3,4,9,10-bis(dicarboxylic anhydride) was synthesized according to a method reported previously in the literature.[40] 1,7-Dibromoperylene-3,4,9,10-bis(dicarboxylic anhydride) was further reacted with *n*-octyl-1-amine was carried out as follows.[41,42] 1,7-Dibromoperylene-3,4,9,10-bis(dicarboxylic anhydride) (1.50 g, 2.6 mmol) in a mixture of *n*-butyl alcohol and deionized water (1:1, v/v, 100 mL) was sonicated for 10 min. Then, *n*-octyl-1-amine (1.03 g, 8.0 mmol) was added and the reaction mixture was stirred at 80 °C for 17 h under nitrogen atmosphere. Concentrated aqueous HCl (10 mL) was added and the mixture was stirred at room temperature for 30 min. The mixture was extracted with chloroform (2 × 100 mL), washed with deionized water (2 × 100 mL), and dried over anhydrous Na_2SO_4. The solvent was removed and the residue was purified by column chromatography over silica gel eluting with dichloromethane, giving the target product PDIC8 in a red solid (1.8 g, 90% yield). The obtained product was identified by ^{1}H NMR spectroscopy. ^{1}H NMR (300 MHz, $CDCl_3$, δ (ppm)): 9.42 (d, J = 8.0 Hz, 2H), 8.91 (s, 2H), 8.68 (d, J = 8.0 Hz, 2H), 4.17 (t, J = 7.50 Hz, 4H), 1.73 (d, J = 7.20 Hz, 4H), 1.28 (s, 20H), 0.88 (t, J = 6.90 Hz, 6H). The ^{1}H NMR data were confirmed to be consistent with those reported previously in the literature.[38,41] The product likely contained a mixture of 1,7- and 1,6-isomers as commonly observed in materials originated from dibromoperylenebis(dicarboxylic anhydride), and was used without separation of the isomers.

Synthesis of Poly([N,N′-dioctylperylene-3,4,9,10-bis(dicarboximide)-1,7(6)-diyl]-alt-[(2,5-bis(2-ethylhexyl)-1,4-phenylene)bis(ethyn-2,1-diyl]) (PDIC8-EB): The above obtained PDIC8 (0.50 g, 0.646 mmol) was weighed into an oven-dried Schlenk flask containing a stir bar. 1,4-Bis(2-ethylhexyl)-2,5-diethynylbenzene (EB)[41] (0.226g, 0.646 mmol) was dissolved in tetrahydrofuran (THF, 5 mL) and added by syringe into the Schlenk vessel under nitrogen. Additional dry THF (5 mL) and triethylamine (5 mL, 3.63 g, 35.9 mmol) were added by syringe. $PdCl_2(PPh_3)_2$ (8.95 mg, 0.0128 mmol) and copper(I) iodide (2.43 mg, 0.0128 mmol) were added to the reaction mixture. The reaction mixture was pump-filled with nitrogen three times, stirred for 15 min at room temperature, and then heated at 90 °C for 3 days (during which time a dark suspension with precipitates was formed). After allowing the mixture to cool to room temperature, it was added dropwise to methanol (ca. 300 mL), and the resulting solid was filtered. The crude product–a blackish solid–was purified by Soxhlet extraction with methanol, acetone, hexane, and chloroform. The chloroform extracts were precipitated into methanol and dried in vacuum, giving PDIC8-EB in a dark solid (530 mg, 0.552 mmol, 85% yield). UV-vis ($CHCl_3$, λ_{max} (nm)): 365, 467, 581, 633 nm. UV-vis (film, λ_{max} (nm)): 365, 475, 582, 634. GPC (after Soxhlet) in $CHCl_3$ (with heating to dissolve the sample): $\overline{M_w}$ = 66 900 Da; PDI = 4.22. ^{1}H NMR ($CDCl_3$, 500 MHz, δ (ppm)): 9.74 (br, 2H), 8.57 (br, 4H), 7.95-7.65 (br, 2H), 4.26 (br, 4H), 2.96 (br, 4H), 2.55-0.88 (br, 60H). Elemental analysis. Calcd. for $C_{66}H_{76}N_2O_4$: C, 82.46%; H, 7.97%; N, 2.91%. Found: C, 81.61%; H, 8.16%; N, 2.91%.

Preparation of Suspension of PDIC8-EB Nanowires: A suspension of PDIC8-EB nanowires was prepared by dissolving the polymer (5–10 mg) in deoxygenated chloroform (1 mL) under nitrogen atmosphere. The mixture was stirred at 80 °C for 24 h to obtain a completely dissolved hot solution and then cooled to room temperature, followed by filtration through polytetrafluoroethylene (PTFE) membrane microfilters with a pore size of 0.2 µm. The filtered suspension was kept at room temperature in the dark for 72 h, during which time its viscosity increased. The suspension was stored in nitrogen atmosphere before used for fabricating OFET devices and/or for characterization purposes.

Measurements: Thermogravimetric analysis (TGA) was conducted at a heating rate of 10 °C min^{-1} under a nitrogen gas flow of 30 mL min^{-1} using a Seiko TG/DTA-6300 thermal analyzer. Differential scanning calorimetry (DSC) was carried out at a heating rate of 10 °C min^{-1} under a nitrogen atmosphere using a TA instruments 2100 calorimeter.

Electrochemical measurements were carried out in dry deoxygenated 0.1 M tetra-*n*-butylammonium hexafluorophosphate in chloroform using a CH Instrument Electrochemical Workstation #A2314 potentiostat and a conventional three-electrode cell with a glassy carbon working electrode, platinum wire counter electrode, and an Ag wire coated with AgCl as the pseudo-reference electrode. Potentials were referenced to ferrocenium/ferrocene by using ferrocene as an internal reference. Cyclic voltammograms were recorded at a scan rate of 50 mV s^{-1}. For a polymer film, it was deposited onto a Pt working electrode by drop casting from a solution (0.1 wt% solid) of the polymer in chloroform and then dried

under vacuum at 80 °C for 2 h and then scanned at a rate of 50 mV s^{-1} in deoxygenated 0.1 M tetra-*n*-butylammonium hexafluorophosphate in acetonitrile. For the polymer film cast onto a heavily doped n^+–Si(100) substrate, the ionization potential (IP) of the polymer was measured by ultraviolet photoelectron spectroscopy (UPS; He-I source, $h\nu = 21.2$ eV) using a VG ESCALAB 220i spectrometer; here, the IP was obtained from a relationship, $IP = h\nu - (E_K^{max} - E_K^{cutoff})$ where E_K^{cutoff} is the inelastic cutoff, at which electrons have just sufficient energy to escape from the solid, and E_K^{max} is the energy of the highest kinetic energy electrons detected, which corresponds to ionization from the highest filled orbital. For the polymer thin films which were spin-coated onto Si substrates at ambient atmosphere at 700 rpm for 40 s and then dried for 24 h in vacuum at room temperature, AFM experiments were carried out in tapping mode at ambient temperature using a microscope (Veeco Instruments SPM 3100). Both topographical and phase images were acquired at the same time. Using an electron microscope (JEOL JEM 2200FS), high resolution TEM analysis was carried out with a working voltage of 200 keV and a point resolution of 0.1 nm on delaminated thin films, which were transferred onto 300 mesh copper grids and then annealed at 200 °C. Exposure time and electron dose were reduced to minimize the possibility of electron-irradition damage; parameters for imaging were also optimized. The samples were dried in vacuum and stored under nitrogen. For the polymer films coated on silicon substrates, synchrotron GIXS measurements were conducted at the 3C and 4C beamlines[43] of the Pohang Accelerator Laboratory (PAL) at Pohang University of Science & Technology (POSTECH). The incident angle α_i of the X-ray beam was set at 0.160°, which is between the critical angles of the films and the silicon substrate ($\alpha_{c,f}$ and $\alpha_{c,s}$). Scattering data were measured at a sample-to-detector distance of 117.2 mm using an X-ray radiation source of 1.38 Å wavelength and a two-dimensional charge-coupled detector (2D CCD) (Mar, USA). All scattering measurements were carried out at 25 °C. Each data set was collected for 30–60 s. Specular XR measurements were carried out at the 3D and 8D beamlines of PAL, POSTECH.[44] Sample specimens were mounted on a Huber four-circle goniometer, and a scintillation counter with an enhanced dynamic range (Bede Scientific, EDR) was used as a detector. The measured intensities were normalized to the intensity of the incident beam which was monitored at an ionization chamber. An X-ray wavelength of 1.54 Å was used.

OFET device fabrication and characterization: BGTC OFET devices were fabricated on heavily doped n^+–Si(100) substrates with a 300-nm-thick thermally grown SiO_2 layer ($C_i = 10$ nF cm^{-2}). The Si/SiO_2 substrates were immersed in a piranha solution (conc. H_2SO_4:H_2O_2 = 7:3 in volume) for 20 min, and were then washed thoroughly using deionized water. The cleaned substrates were immediately treated with HMDS or OTS-C8 to form a self-assembled monolayer (SAM). Neat HMDS was spin-coated at 4000 rpm for 30 s, while an OTS-C8 monolayer was formed by immersing the substrate in its toluene solution for 2 h. All coated substrates were annealed at 120 °C for 30 min in ambient air. For each device, the active polymer layer was prepared by spin-coating of its suspension with a concentration of 5 mg mL^{-1} at 1500 rpm for 40 s in a nitrogen atmosphere and subsequent drying at room temperature under vacuum for 12 h. Gold source and drain electrodes with a thickness of 100 nm were deposited at a rate of ca 1.5 nm s^{-1} in vacuum through a shadow mask, giving source-drain channels with a length L of 100 μm and a width W of 1500 μm. In addition, BGBC OFET devices were prepared with source-drain channels in a size of $L = 40$ μm and $W = 800$ μm (see the fabrication details in the Supporting Information). For the prepared devices, electrical characteristics were measured before and after thermal annealing for 1 h at a chosen temperature over 25–240 °C. The thermal annealing process was carried out on a hot plate inside a nitrogen-purged glove box (H_2O and O_2 concentration < 0.1 ppm). All device fabrication processes and tests were conducted in dark condition under nitrogen atmosphere. Current–voltage characteristics were measured at room temperature in a nitrogen atmosphere using a Keithley 4200-SCS semiconductor characterization system. Field-effect electron mobility μ_e was determined in the saturation regime ($V_{sd} = 80$ V) using an equation, $I_{sd} = \mu_e(W/2L)C_i(V_g - V_t)^2$ where C_i is the capacitance of the SiO_2 dielectric, I_{sd} is the source-drain current, and V_{sd}, V_g, and V_t are the source-drain, gate, and threshold voltages, respectively. Current on/off ratios (I_{on}/I_{off}) were determined from the current at $V_g = 80$ V (I_{on}) and the minimum current at $V_g \approx -20$ to 3 V (I_{off}). In addition, field-effect electron mobility $\mu_{e,l}$ in the linear regime (particularly at $V_{sd} = 3.0$ V) was determined by analysis of data (which were extracted from the output curves of devices) using an equation, $I_{sd} = \mu_{e,l}(W/L)C_i(V_g - V_t)V_{sd}$.

Supporting Information

Supporting Information is available from the Wiley Online Library or from the author.

Acknowledgements

S.G.H., Y.R., and J.J. contributed equally to this work. This work was supported by the STC Program of the National Science Foundation (DMR-0120967), Solvay SA, the National Research Foundation (NRF) of Korea (Doyak Program 2011-0028678 and Center for Electro-Photo Behaviors in Advanced Molecular Systems (2010-0001784)), and by the Ministry of Education, Science & Technology (MEST), Korea (BK21 Program and World Class University Program (R31-2008-000-10059-0)). Synchrotron GIXS and XR measurements were supported by MEST, POSCO and POSTECH Foundation. The authors thank Dr. Nam-Suk Lee at National Center for Nanomaterials Technology (NCNT) at POSTECH for high resolution TEM measurements. Drs. Richard Mason, Benjamin Wunch, and Mariacristina Rumi are gratefully acknowledged for monomer synthesis, calorimetry analysis, and valuable discussions respectively.

Received: July 24, 2012
Revised: October 8, 2012
Published online: November 20, 2012

[1] H. Sirringhaus, P. J. Brown, R. H. Friend, M. M. Nielsen, K. Bechgaard, B. M. W. Langeveld-Voss, A. J. H. Spiering, R. A. J. Janssen, E. W. Meijer, P. Herwig, D. M. de Leeuw, *Nature* **1999**, *401*, 685.
[2] A. L. Briseno, S. C. B. Mannsfeld, M. M. Ling, S. Liu, R. J. Tseng, C. Reese, M. E. Roberts, Y. Yang, F. Wudl, Z. Bao, *Nature* **2006**, *444*, 913.
[3] M. Muccini, *Nat. Mater.* **2006**, *5*, 605.
[4] J. Zaumseil, R. H. Friend, H. Sirringhaus, *Nat. Mater.* **2006**, *5*, 69.
[5] C. Kim, A. Facchetti, T. J. Marks, *Science* **2007**, *318*, 76.
[6] D. J. Gundlach, *Nat. Mater.* **2008**, *7*, 216.
[7] C. D. Dimitrakopoulos, *Science* **1999**, *283*, 822.
[8] A. Dodabalapur, H. E. Katz, L.Torsi, R. C. Haddon, *Science* **1995**, *269*, 1560.
[9] I. N. Hulea, *Nat. Mater.* **2006**, *5*, 982.
[10] a) H. Sirringhaus, *Adv. Mater.* **2005**, *17*, 2411; b) H. E. Katz, *Chem. Mater.* **2004**, *16*, 4748.
[11] Z. Bao, A. Dodabalapur, A. J. Lovinger, *Appl. Phys. Lett.* **1996**, *69*, 4108.
[12] H. Sirringhaus, N. Tessler, R. H. Friend, *Science* **1998**, *280*, 1741.
[13] J. Veres, S. Ogier, G. Lloyd, D. de Leeuw, *Chem. Mater.* **2004**, *16*, 4543.
[14] E. Lim, Y. M. Kim, J.-I. Lee, B.-J. Jung, N. S. Cho, J. Lee, L.-M. Do, H.-K. Shim, *J. Polym. Sci., Polym. Chem. Ed.* **2006**, *44*, 4709.
[15] I. McCulloch, M. Heeney, C. Bailey, K. Genevicius, I. MacDonald, M. Shkunov, D. Sparrowe, S. Tierney, R. Wagner, W. Zhang,

M. L. Chabinyc, R. J. Kline, M. D. McGehee, M. F. Toney, *Nat. Mater.* **2006**, *5*, 328.

[16] B. S. Ong, Y. Wu, P. Liu, S. Gardner, *J. Am.Chem. Soc.* **2004**, *126*, 3378.

[17] I. Osaka, K. Takimiya, R. D. McCullough, *Adv. Mater.* **2010**, *22*, 4993.

[18] a) X. Guo, F. S. Kim, S. A. Jenekhe, M. D. Watson, *J. Am. Chem. Soc.* **2009**, *131*, 7206; b) I. McCulloch, M. Heeney, M. L. Chabinyc, D. DeLongchamp, R. J. Kline, M. Cölle, W. Duffy, D. Fischer, D. Gundlach, B. Hamadani, R. Hamilton, L. Richter, A. Salleo, M. Shkunov, D. Sparrowe, S. Tierney, W. Zhang, *Adv. Mater.* **2009**, *21*, 1091; c) W. Zhang, J. Smith, S. E. Watkins, R. Gysel, M. McGehee, A. Salleo, J. Kirkpatrick, S. Ashraf, T. Anthopoulos, M. Heeney, I. McCulloch, *J. Am. Chem. Soc.* **2010**, *132*, 11437; d) T. Umeda, D. Kumaki, S. Tokito, *J. Appl. Phys.* **2009**, *105*, 024516; e) H. Bronstein, Z. Chen, R. S. Ashraf, W. Zhang, J. Du, J. R. Durrant, P. S. Tuladhar, K. Song, S. E. Watkins, Y. Geerts, M. M. Wienk, R. A. J. Janssen, T. Anthopoulos, H. Sirringhaus, M. Heeney, I. McCulloch, *J. Am. Chem. Soc.* **2011**, *133*, 3272; f) J. Mei, D. H. Kim, A. L. Ayzner, M. F. Toney, Z. Bao, *J. Am. Chem. Soc.* **2011**, *133*, 20130; g) H. N. Tsao, D. M. Cho, I. Park, M. R. Hansen, A. Mavrinskiy, D. Y. Yoon, R. Graf, W. Pisula, H. W. Spiess, K. Müllen, *J. Am. Chem. Soc.* **2011**, *133*, 2605; h) H. Chen, Y. Guo, G. Yu, Y. Zhao, J. Zhang, D. Gao, H. Liu, Y. Liu, *Adv. Mater.* **2012**, *24*, 4618.

[19] J. A. Letizia, M. R. Salata, C. M. Tribout, A. Facchetti, M. A. Ratner, T. J. Marks, *J. Am. Chem. Soc.* **2008**, *130*, 9679.

[20] A. Babel, S. A. Jenekhe, *J. Am. Chem. Soc.* **2003**, *125*, 13656.

[21] Z. Chen, Y. Zheng, H.Yan, A. Facchetti, *J. Am. Chem. Soc.* **2009**, *131*. 8.

[22] H. Yan, Z. Chen, Y. Zheng, C. Newman, J. R. Quinn, F. Dotz, M. Kastler, A. Facchetti, *Nature* **2009**, *457*, 679.

[23] X. Guo, F. S. Kim, M. J. Seger, S. A. Jenekhe, M. D. Watson, *Chem. Mater.* **2012**, *24*, 1434.

[24] X. Zhan, Z. A. Tan, B. Domercq, Z. An, X. Zhang, S. Barlow, Y. Li, D. Zhu, D. B. Kippelen, S. R Marder, *J. Am. Chem. Soc.* **2007**, *129*, 7246.

[25] a) S. Huttner, M. Sommer, M. Thelakkat, *Appl. Phys. Lett.* **2008**, *92*, 093302; b) X. Zhao, X. Zhan, *Chem. Soc. Rev.* **2011**, *40*, 3728; c) W. Zhou, Y. Wen, L. Ma, Y. Liu, X. Zhan, *Macromolecules*, **2012**, *45*, 4115.

[26] H. Usta, A. Facchetti, T. J. Marks, *J. Am. Chem. Soc.* **2008**, *130*, 8580.

[27] J. E. Anthony, A. Facchetti, M. Heeney, S. R. Marder, X. Zhan, *Adv. Mater.* **2010**, *22*, 3876.

[28] a) F. S. Kim, G. Ren, S. A. Jenekhe, *Chem. Mater.* **2011**, *23*, 682; b) A. Babel, D. Li, Y. Xia, S. A. Jenekhe, *Macromolecules* **2005**, *38*, 4705; c) S. B. Jo, W. H. Lee, L. Qiu, K. Cho, *J. Mater. Chem.* **2012**, *22*, 4244.

[29] a) J. A. Merlo, C. D. Frisbie, *J. Phys. Chem. B* **2004**, *108*, 19169; b) H. Yang, T. J. Shin, L. Yang, K. Cho, C. Y. Ryu, Z. Bao, *Adv. Funct. Mater.* **2005**, *15*, 671.

[30] A. L. Briseno, S. C. B. Mannsfeld, P. J. Shamberger, F. S. Ohuchi, Z. Bao, S. A. Jenekhe, Y. Xia, *Chem. Mater.* **2008**, *20*, 4712.

[31] M. M. Durban, P. D. Kazarinoff, Y. Segawa, C. K. Luscombe, *Macromolecules* **2011**, *33*, 4721.

[32] T. Sajoto, S. P. Tiwari, H. Li, C. Risko, S. Barlow, Q. Zhang, J.-Y. Cho, J. L. Brédas, B. Kippelen, S. R. Marder, *Polymer* **2012**, *53*, 1072.

[33] a) C. Huang, S. Barlow, S. R. Marder, *J. Org. Chem.* **2011**, *76*, 2386; b) X. Zhan, A. Facchetti, S. Barlow, T. J. Marks, M. A. Ratner, M. R. Wasielewski, S. R. Marder, *Adv. Mater.* **2011**, *23*, 268.

[34] X. Zhan, Z. Tan, E. Zhou, Y. Li, R. Misra, A. Grant, B. Domercq, X. Zhang, Z. An, X. Zhang, S. Barlow, B. Kippelen, S. R. Marder, *J. Mater. Chem.* **2009**, *19*, 5794.

[35] J. Yoon, K. S. Jin, H. C. Kim, G. Kim, K. Heo, S. Jin, J. Kim, K.-W. Kim, M. Ree, *J. Appl. Crystallogr.* **2007**, *40*, 476.

[36] P. G. de Gennes, J. Prost, *The Physics of Liquid Crystals*. Oxford University Press, New York **1993**.

[37] a) L. G. Parratt, *Phys. Rev.* **1954**, *95*, 359; b) J. Bolze, M. Ree, H. S. Youn, S.-H. Chu, K. Char, *Langmuir* **2001**, *17*, 6683; c) Y. Hwang, K. Heo, C. H. Chang, M. K. Joo, M. Ree, *Thin Solid Films* **2006**, *510*, 159; d) S. Park, K. Kim, D. M. Kim, W. Kwon, J. Choi, M. Ree, *ACS Appl. Mater. Interfaces* **2011**, *3*, 765; e) Y.-G. Ko, W. Kwon, D. M. Kim, Y.-S. Gal, M. Ree, *Polym. Chem.* **2012**, *3*, 2028; f) Y.-G. Ko, W. Kwon, H.-J. Yen, C.-W. Chang, D. M. Kim, K. Kim, S. G. Hahm, T. J. Lee, G.-S. Liou, M. Ree, *Macromolecules* **2012**, *45*, 3749.

[38] B. J. Jones, A. Facchetti, M. R. Wasielewski, T. J. Marks, *J. Am. Chem. Soc.* **2007**, *129*, 15259.

[39] A. L. Briseno, F. S. Kim, A. Babel, S. A. Jenekhe, Y. Xia, *J. Mater. Chem.* **2011**, *21*, 16461.

[40] F. Wurthner, V. Stepanenko, Z. Chen, C. R. Saha-Moller, N. Kocher, N. D. Stalke, *J. Org. Chem.* **2004**, *69*, 7933.

[41] U. Rohr, C. Kohl, K. Müllen, A. van de Craats, J. Warman, *J. Mater. Chem.* **2001**, *11*, 1789-1799.

[42] D. A. M. Egbe, S. Sell, C. Ulbricht, E. Birckner, U.-W. Grummt, *Macromol. Chem. Phys.* **2004**, *205*, 2105.

[43] a) J. Bolze, J. Kim, J.-Y. Huang, S. Rah, H. S. Youn, B. Lee, T. J. Shin, M. Ree, *Macromol. Res.* **2002**, *10*, 2; b) J. Yoon, K.-W. Kim, J. Kim, K. Heo, K. S. Jin, S. Jin, T. J. Shin, B. Lee, Y. Rho, B. Ahn, M. Ree, *Macromol. Res.* **2008**, *16*, 575; c) B. Lee, Y.-H. Park, Y. Hwang, W. Oh, J. Yoon, M. Ree, *Nat. Mater.* **2005**, *4*, 147; d) B. Lee, W. Oh, Y. Hwang, Y.-H. Park, J. Yoon, K. S. Jin, K. Heo, J. Kim, K.-W. Kim, M. Ree, *Adv. Mater.* **2005**, *17*, 696; e) J. Jung, J. C. Kim, Y. Rho, M. Kim, H. Kim, M. Ree, *ACS Appl. Mater. Interfaces* **2011**, *3*, 2655; f) W. Kwon, Y. Rho, K. Kamoshida, K. H. Kwon, Y. C. Jeong, J. Kim, H. Misaka, T. J. Shin, J. Kim, K.-W. Kim, K. S. Jin, T. Chang, H. Kim, T. Satoh, T. Kakuchi, M. Ree, *Adv. Funct. Mater.* **2012**, DOI: 10.1002/adfm.201201101.

[44] a) B.-J. Park, S.-Y. Rah, Y.-J.Park, K.-B. Lee, *Rev. Sci. Instrum.* **1995**, *66*, 1722; b) Y.-G. Ko, W. Kwon, H.-J. Yen, C.-W. Chang, D. M. Kim, K. Kim, S. G. Hahm, T. J. Lee, G.-S. Liou, M. Ree, *Macromolecules* **2012**, *45*, 3749; c) T. J. Lee, Y.-G. Ko, H.-J. Yen, K. Kim, D. M. Kim, W. Kwon, S. G. Hahm, G.-S. Liou, M. Ree, *Polym. Chem.* **2012**, *3*, 1276; d) S. G. Hahm, T. J. Lee, D. M. Kim, W. Kwon, Y.-G. Ko, T. Michinobu, M. Ree, *J. Phys. Chem. C* **2011**, *115*, 21954.